
Extragalactic Compact Sources in the *Planck* Sky and Their Cosmological Implications

Luigi Toffolatti, Carlo Burigana,
Francisco Argüeso and José M. Diego

Additional information is available at the end of the chapter

<http://dx.doi.org/10.5772/52908>

1. Introduction

As of mid August 2012, the *Planck* cosmic microwave background anisotropy probe¹ [1,2] – launched into space on 14 May 2009 at 13:12:02 UTC, by an Ariane 5 ECA launcher, from the Guiana Space Centre, Kourou, French Guiana – is still successfully operating. The spacecraft accumulated data with its two instruments, the High Frequency Instrument (HFI) [3], based on bolometers working between 100 and 857 GHz, and the Low Frequency Instrument (LFI) [4], based on radiometers working between 30 and 70 GHz, up to the consumption of the cryogenic liquids on January 2012, achieving $\simeq 29.5$ months of integration, corresponding to about five complete sky surveys. A further 12 months extension is on-going for observations with LFI only, cooled down with the cryogenic system provided by HFI. Moreover, *Planck* is sensitive to linear polarization up to 353 GHz.

Thanks to its great sensitivity and resolution on the whole sky and to its wide frequency coverage that allows a substantial progress in foreground modeling and removal, *Planck* will open a new era in our understanding of the Universe and of its astrophysical structures (see [5] for a full description of the *Planck* Scientific programme). *Planck* will improve the accuracy of current measures of a wide set of cosmological parameters by a factor from ~ 3 to ~ 10 and will characterize the geometry of the Universe with unprecedented accuracy. *Planck* will shed light on many of the open issues in the connection between the early stages of the Universe and the evolution of the cosmic structures, from the characterization of primordial conditions and perturbations, to the late phases of cosmological reionization.

* This paper is based largely on the *Planck* Early Release Compact Source Catalogue, a product of ESA and the *Planck* Collaboration. Any material presented in this review that is not already described in *Planck* Collaboration papers represents the views of the authors and not necessarily those of the *Planck* Collaboration.

¹ *Planck* (<http://www.esa.int/Planck>) is a project of the European Space Agency - ESA - with instruments provided by two scientific Consortia funded by ESA member states (in particular the lead countries: France and Italy) with contributions from NASA (USA), and telescope reflectors provided in a collaboration between ESA and a scientific Consortium led and funded by Denmark.

The *Planck* perspectives on some crucial selected topics linking cosmology to fundamental physics (the neutrino masses and effective number of species, the primordial helium abundance, various physics fundamental constants, the parity property of CMB maps and its connection with CPT symmetry with emphasis to the Cosmic Birefringence, the detection of the stochastic field of gravitational waves) will also show how *Planck* represents an extremely powerful *fundamental and particle physics laboratory*. Some of these analyses will be carried out mainly through a precise measure of CMB anisotropy angular power spectrum (APS) in temperature, polarization and in their correlations, whereas others, in particular those related to the geometry of the Universe and to the research of non-Gaussianity signatures, are based on the exploitation of the anisotropy pattern. The most ambitious goal is the possible detection of the so-called B-mode APS.

The first scientific results², the so-called *Planck* Early Papers³ have been released in January 2011 and published by Astronomy and Astrophysics (EDP sciences), in the dedicated Volume 536 (December 2011). A further set of astrophysical results has been presented on the occasion of the Conference *Astrophysics from radio to sub-millimeter wavelengths: the Planck view and other experiments*⁴ held in Bologna on 13-17 February 2012. Several articles have been already submitted in 2012 and others are in preparation, constituting the set of so-called *Planck* Intermediate Papers.

The outline of this Chapter is as follows: in Section 2 we briefly sketch the main characteristics and the capabilities of the ESA *Planck* mission; in Section 3 we discuss the most recent detection methods for compact source detection; in Section 4 the SZ effect, detected by *Planck* in many cluster of galaxies and its importance for cosmological studies are analyzed; Section 5 is dedicated to summarize current results obtained by *Planck* data on the properties of EPS; finally, Section 6, discusses the very important results up to now achieved by the analysis of CIB anisotropies detected by *Planck*.

2. The ESA *Planck* mission: Overview

CMB experimental data are affected by uncertainties due to instrumental noise (crucial at high multipoles, ℓ , i.e. small angular scales), cosmic and sampling variance (crucial at low ℓ , i.e. large angular scales) and from systematic effects. The uncertainty on the angular power spectrum is given by the combination of three components, cosmic and sampling variance, and instrumental noise, and it is approximately given by [9]:

$$\frac{\delta C_\ell}{C_\ell} = \sqrt{\frac{2}{f_{sky}(2\ell+1)}} \left(1 + \frac{A\sigma^2}{NC_\ell W_\ell} \right). \quad (1)$$

Here f_{sky} is the sky coverage, A is the surveyed area, σ is the instrumental rms noise per pixel, N is the total pixel number, W_ℓ is the beam window function that, in the case of

² http://www.sciops.esa.int/index.php?project=PLANCK&page=Planck_Published_Papers

³ The *Planck* Early papers describe the instrument performance in flight including thermal behaviour (papers I-IV), the LFI and HFI data analysis pipelines (papers V-VI), and the main astrophysical results (papers VII-XXVI). These papers have complemented by a subsequent work, published in 2012, based on a combination of high energy and *Planck* observations (see [8]).

⁴ <http://www.iasfbo.inaf.it/events/planck-2012/>

LFI				HFI		
Frequency (GHz)	30	44	70	Frequency (GHz)	100	143
FWHM	33.34	26.81	13.03	FWHM in T (P)	9.6 (9.6)	7.1 (6.9)
N of R (or feeds)	4 (2)	6 (3)	12 (6)	N of B in T (P)	– (8)	4 (8)
EB	6	8.8	14	EB in T (P)	33 (33)	43 (46)
NET	159	197	158	NET in T (P)	100 (100)	62 (82)
$\delta T/T$ [$\mu K/K$] (in T)	2.04	3.14	5.17	$\delta T/T$ [$\mu K/K$] (in T)	2.04	1.56
$\delta T/T$ [$\mu K/K$] (in P)	2.88	4.44	7.32	$\delta T/T$ [$\mu K/K$] (in P)	3.31	2.83
HFI			HFI			
Frequency (GHz)	217	353	Frequency (GHz)	545	857	
FWHM in T (P)	4.6 (4.6)	4.7 (4.6)	FWHM in T	4.7	4.3	
N of B in T (P)	4 (8)	4 (8)	N of B in T	4	4	
EB in T (P)	72 (63)	99 (102)	EB in T	169	257	
NET in T (P)	91 (132)	277 (404)	NET in T	2000	91000	
$\delta T/T$ [$\mu K/K$] in T (P)	3.31 (6.24)	13.7 (26.2)	$\delta T/T$ [$\mu K/K$] in T	103	4134	

Table 1. *Planck* performance. The average sensitivity, $\delta T/T$, per $(FWHM)^2$ resolution element (FWHM: Full Width at Half Maximum of the beam response function, is indicated in arcmin) is given in CMB temperature units (i.e., equivalent thermodynamic temperature) for 29.5 (plus 12 for LFI) months of integration. The white noise (per frequency channel for LFI and per detector for HFI) in 1 sec of integration (NET, in $\mu K \cdot \sqrt{s}$) is also given in CMB temperature units. The other acronyms here used are: N of R (or B) = number of radiometers (or bolometers), EB = effective bandwidth (in GHz). Adapted from [6, 7] and consistent with [3, 4]. Note that at 100 GHz all bolometers are polarized and the equivalent temperature value is obtained by combining polarization measurements.

a Gaussian symmetric beam, is $W_\ell = \exp(-\ell(\ell + 1)\sigma_B^2)$, with $\sigma_B = FWHM/\sqrt{8 \ln 2}$ the beamwidth which defines the angular resolution of the experiment. For $f_{sky} = 1$ the first term in parenthesis defines the “cosmic variance”, an intrinsic limit on the accuracy at which the APS of a certain cosmological model defined by a suitable set of parameters can be derived with CMB anisotropy measurements⁵. It typically dominates the uncertainty on the APS at low ℓ because of the small, $2\ell + 1$, number of modes m for each ℓ . The second term in parenthesis characterizes the instrumental noise, that never vanishes in the case of real experiments. Note also the coupling between experiment sensitivity and resolution, the former defining the low ℓ experimental uncertainty, namely for W_ℓ close to unit, the latter determining the exponential loss in sensitivity at angular scales comparable with the beamwidth. We computed an overall sensitivity value, weighted over the channels, defined by $1/\sigma_j^2 = \sum_i 1/\sigma_{ji}^2$, where $j = T$ and i indicates the sensitivity of each frequency channel, listed in Table 1. FWHM values of 13 and 33 arcmin are used in Fig.1 to define the overall combination of *Planck* sensitivity and resolution, i.e. the computation of the effective beam window function⁶, relevant for the sensitivity at high ℓ . Finally, to improve the signal to noise ratio in the APS sensitivity, especially at high multipoles, a multipole binning is usually applied. Of course, the real sensitivity of the whole mission will have to also include the potential residuals of systematic effects. The *Planck* mission has been designed to suppress

⁵ Note that the cosmic and sampling variance (74% sky coverage excluding the sky regions mostly affected by Galactic emission) implies a dependence of the overall sensitivity on r at low multipoles, relevant to the parameter estimation; instrumental noise only determines the capability of detecting the B mode.

⁶ In fact, it is possible to smooth maps acquired at higher frequencies with smaller beamwidths to the lowest resolution corresponding to a given experiment. We adopt here FWHM values of 33 and 13 arcmin, which correspond to the lowest resolution of all the *Planck* instruments (i.e., 30 GHz channel) and to the lowest resolution of the so called cosmological channels (i.e., 70 GHz channel), respectively (see Table 1).

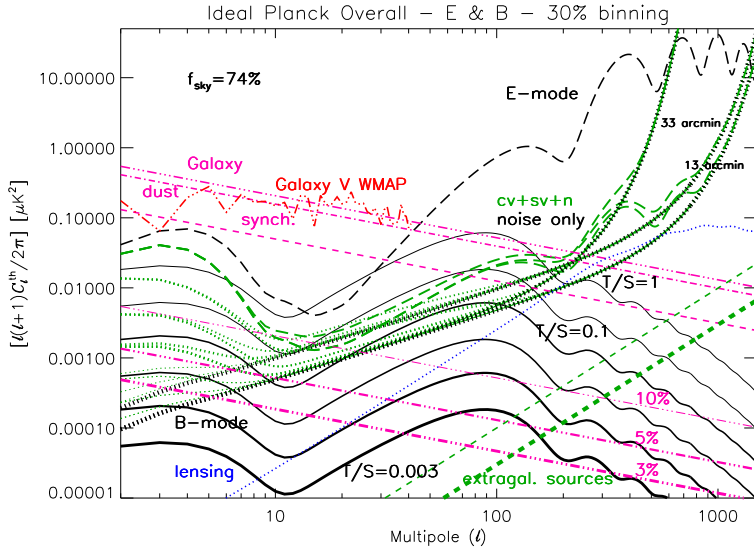


Figure 1. CMB E polarization modes (black long dashes) compatible with *WMAP* data and CMB B polarization modes (black solid lines) for different tensor-to-scalar ratios $T/S = r$ of primordial perturbations are compared to the *Planck* overall sensitivity to the APS assuming two different FWHM angular resolutions (33 and 13 arcmin) and the overall sensitivity corresponding to the whole mission duration (and also to two surveys only: upper curve in black thick dots, labeled 13 arcmin). The expected noise is assumed to be properly subtracted. The plots include cosmic and sampling variance plus instrumental noise (green dots for B modes, green long dashes for E modes, labeled with $cv+sv+n$; black thick dots, noise only) assuming a multipole binning of 30%. The B mode induced by lensing (blue dots) is also shown. Galactic synchrotron (purple dashes) and dust (purple dot-dashes) polarized emissions produce the overall Galactic foreground (purple three dot-dashes). *WMAP* 3-yr power-law fits for uncorrelated dust and synchrotron have been used. For comparison, *WMAP* 3-yr results (<http://lambda.gsfc.nasa.gov/>) derived from the foreground maps using HEALPix tools (<http://healpix.jpl.nasa.gov/>) [12] are shown (red three dot-dashes broken line): power-law fits provide (generous) upper limits to the power at low multipoles. Residual contamination levels by Galactic foregrounds (purple three dot-dashes) are shown for 10%, 5%, and 3% of the map level, at increasing thickness. We plot also as thick and thin green dashes realistic estimates of the residual contribution of un-subtracted extragalactic sources, $C_\ell^{\text{res,PS}}$ and the corresponding uncertainty, $\delta C_\ell^{\text{res,PS}}$.

potential systematic effects down to $\sim \mu K$ level or below. Fig.1 compares CMB polarization modes with the ideal sensitivity of *Planck* (including also a 15% level of HFI data loss because of cosmic rays; see [10]) and the signals coming from astrophysical foregrounds as discussed below.

CMB anisotropy maps are contaminated by a significant level of foreground emission of both Galactic and extragalactic origin. For polarization, the most critical Galactic foregrounds are certainly synchrotron and thermal dust emission, whereas free-free emission gives a negligible contribution. Other components, like spinning dust and “haze”, are still poorly known, particularly in polarization. Synchrotron emission is the dominant Galactic foreground signal at low frequencies, up to ~ 60 GHz, where dust emission starts to dominate. External galaxies are critical only at high ℓ , and extragalactic radio sources are likely the most crucial in polarization up to frequencies ~ 200 GHz, the most suitable for CMB anisotropy experiments. We parameterize a potential residual from non perfect cleaning of CMB maps from Galactic foregrounds simply assuming that a certain fraction

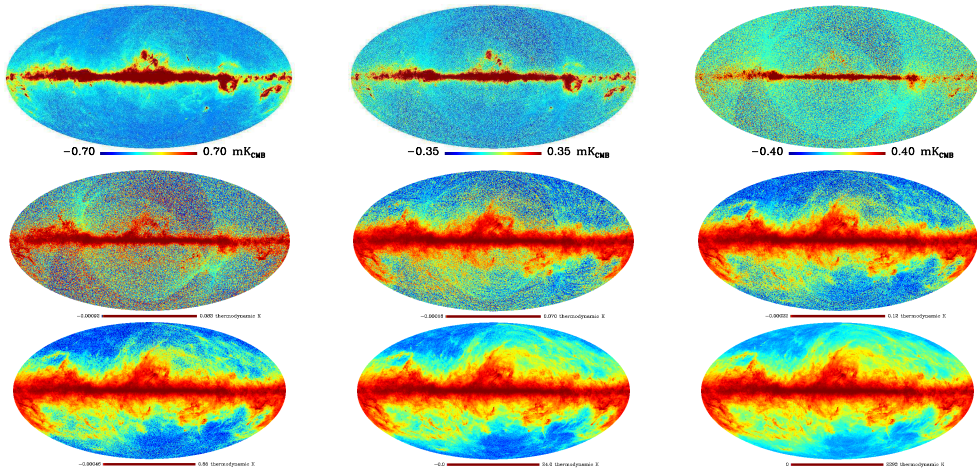


Figure 2. CMB removed *Planck* full-sky maps. From left to right and from top to bottom: 30, 44, 70; 100, 143, 217; 353, 545, and 857 GHz, respectively. Credits: Zacchei, et al., *A&A*, Vol. 536, A5, 2011; *Planck* HFI Core Team, *A&A*, Vol. 536, A6, 2011b, reproduced with permission © ESO.

of the foreground signal *at map level* (or, equivalently, its square at power spectrum level) contaminates CMB maps. Of course, one can easily rescale the following results to any fraction of residual foreground contamination. The frequency of 70 GHz, i.e. the *Planck* channel where Galactic foregrounds are expected to be at their minimum level, at least at angular scales above \sim one degree, is adopted as reference.

For what concerns CMB temperature fluctuations produced by undetected EPS [13], we adopt the recent (conservative) estimate of their Poisson contribution to the (polarized) APS [14] at 100 GHz⁷ by assuming a detection threshold of $\simeq 0.1$ Jy. We also assume a potential residual coming from an uncertainty in the subtraction of this contribution computed by assuming a relative uncertainty of $\simeq 10\%$ in the knowledge of their degree of polarization and in the determination of the source detection threshold, implying a reduction to $\simeq 30\%$ of the original level. Except at very high multipoles, their residual is likely significantly below that coming from Galactic foregrounds.

The first publications of the main cosmological (i.e. properly based on *Planck* CMB maps) implications are expected in early 2013, together with the delivery of a first set of *Planck* maps and cosmological products coming from the first 15 months of data. They will be mainly based on temperature data. Waiting for these products, a first multifrequency view of the *Planck* astrophysical sky has been presented in the Early Papers: Fig. 2 reports the first LFI and HFI frequency (CMB subtracted) maps. These maps are the basis of the construction of the *Planck* Early Release Compact Source Catalog (ERCSC) (see [15] and *The Explanatory Supplement to the Planck Early Release Compact Source Catalogue*), the first *Planck* product delivered to the scientific community.

⁷ We adopt here a frequency slightly larger than that considered for Galactic foregrounds (70 GHz) because at small angular scales, where point sources are more critical, the minimum of foreground contamination is likely shifted to higher frequencies.

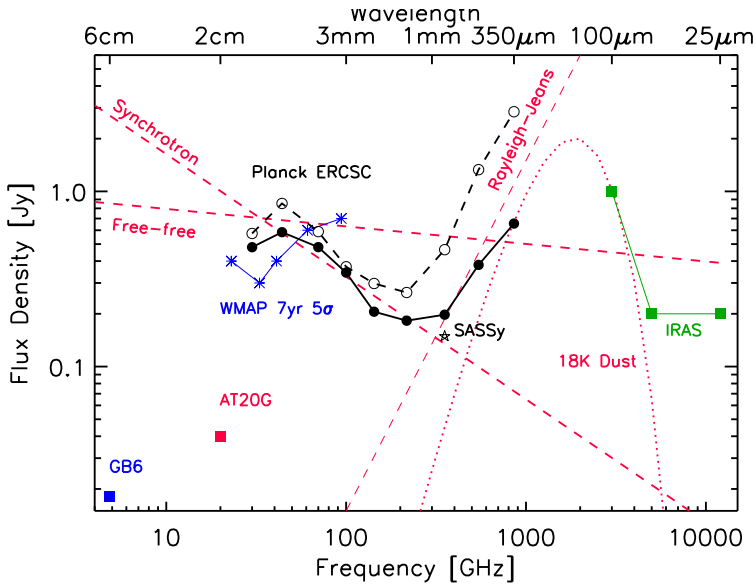


Figure 3. The *Planck* ERCSC flux density limit quantified as the faintest ERCSC sources at $|b| < 10^\circ$ (dashed black line) and at $|b| > 30^\circ$ (solid black line) is shown relative to other wide area surveys. See Fig. 5 of [15] for more details. Credit: *Planck* Collaboration, *A&A*, vol. 536, A7, 2011, reproduced with permission © ESO.

Fig. 3 compares the sensitivity of *Planck* ERCSC with those of other surveys from radio to far-infrared wavelengths. Of course, by accumulating sky surveys and refining data analysis, the *Planck* sensitivity to point sources will significantly improve in the coming years. The forthcoming *Planck* Legacy Catalog of Compact Sources (PCCS), to be released in early 2013 and to be updated in subsequent years, will represent one of the major *Planck* products relevant for multi-frequency studies of compact or point-like sources.

2.1. Extragalactic point sources vs. non-Gaussianity

The cosmological evolution of extragalactic sources and its implications for the CMB and the CIB will be discussed in the following Sections, 5 and 6. On the other hand, statistical analyses of the extragalactic source distribution in the sky can be applied to test cosmological models. In this context, the possibility of probing the Gaussianity of primordial perturbations appears particularly promising. Primordial perturbations at the origin of the large scale structure (LSS) may leave their imprint in the form of small deviations from a Gaussian distribution, [16, 17] that can appear in different kinds of configurations, such as the so-called local type, equilateral, enfolded, orthogonal. For example, the local type of deviation from Gaussianity is parameterized by a constant dimensionless parameter f_{NL} (see, e.g., [18–20]) $\Phi = \phi + f_{NL}(\phi^2 - \langle \phi^2 \rangle)$, where Φ denotes Bardeen’s gauge-invariant potential (evaluated deep in the matter era in the CMB convention) and ϕ is a Gaussian random field. Extragalactic radio sources are particularly interesting as tracers of the LSS since they span large volumes extending out to substantial redshifts. The radio sources from the

NRAO VLA Sky Survey (NVSS), the quasar catalogue of Sloan Digital Sky Survey Release Six (SDSS DR6 QSOs) and the MegaZ-LRG (DR7), the final SDSS II Luminous Red Galaxy (LRG) photometric redshift survey, have been recently analysed by [21] (see this work and references therein for a thorough analysis on the subject). Through a global analysis of the constraints on the amplitude of primordial non-Gaussianity by the angular power spectra obtained from extragalactic radio sources (mapped by these surveys) and, moreover, from their cross-correlation power spectra with the WMAP CMB temperature map, [21] set limits on $f_{NL} = 48 \pm 20$, $f_{NL} = 50 \pm 265$ and $f_{NL} = 183 \pm 95$ at 68% confidence level for local, equilateral and enfolded templates, respectively. These results have been found to be stable with respect to potential systematic errors: the source number density and the contamination by Galactic emissions, for NVSS sources; the use of different CMB temperature fluctuation templates and the contamination of stars in the SDSS and LRG samples. Such tests of non-Gaussianity would have profound implications for inflationary mechanisms – such as single-field slow roll, multifields, curvaton (local type) – and for models which have effects on the halo clustering can be described by the equilateral template (related to higher-order derivative type non-Gaussianity) and by the enfolded template (related to modified initial state or higher-derivative interactions). Fundamental progress on this topic will be achieved by combining forthcoming LSS surveys with the CMB maps provided by *Planck*.

3. Methods for compact source detection in CMB maps

Compact sources, in CMB literature, are defined as spatially bounded sources which subtend very small angular scales in the images, such as galaxies and galaxy clusters. On the other hand, diffuse components, such as the CMB itself and Galactic foregrounds, do not show clear spatial boundaries and extend over large areas of the sky. Due to the fact that compact sources are spatially localized, the techniques for detecting them differ from those applied for the separation of the diffuse components. Most of the detection methods use scale diversity, i.e. different power at different angular scales, to enhance compact sources against diffuse components. Sources must be detected against a combination of CMB, instrumental noise and Galactic foregrounds. From the point of view of signal processing, the source is the signal and the other components are the noise.

Point sources are “compact” sources in the sense that their typical observed angular size is much smaller than the beam resolution of the experiment. Therefore, they appear as point-like objects convolved with the instrumental beam. Radio sources and far-IR sources are usually seen as point-like sources. Galaxy clusters, which are detected through the thermal SZ effect [22], have a shape that is obtained as the convolution of the instrumental beam with the cluster profile. In contrast to point sources, the cluster profile has to be taken into account for cluster detection. However, since the projected angular scale of clusters is generally small, techniques that are useful for point sources can be adapted for clusters, too.

The thermal SZ effect has a general dependence with frequency, that makes the use of multichannel images very convenient for cluster detection. On the contrary, the flux of each individual point source has its own frequency dependence. Despite this fact, the combination of several channels can also improve point source detection. We will review techniques applied to single-frequency channels in a first subsection and then we will discuss more recent methods, that use multichannel information.

3.1. Single channel detection

We now focus on techniques for detecting point-like sources. Galaxy clusters can be detected by similar methods, but taking into account the cluster profile (see, e.g., [23-25]). Since multichannel methods for cluster detection improve significantly the performance of single channel techniques, we leave a more detailed study of clusters for the next subsection.

As mentioned before, compact source detection techniques make use of scale diversity. For example, SEXTRACTOR [26] – where maps are pre-filtered by a Gaussian kernel the same size as the beam – approximates the image background by a low-order polynomial and then subtracts the background from the image. The object is detected after connecting the pixels above a given flux density threshold. SEXTRACTOR has been used for elaborating the *Planck* ERCSC [15] in the highest frequency channels, from 217 to 857 GHz. However, CMB emission and diffuse foregrounds are complex and cannot be modeled in a straightforward way. Thus, apart from this important application, SEXTRACTOR has had a limited use in CMB astronomy.

A standard method which has been used often for compact source detection is the common matched filter (MF) [27]. The MF is just a linear filter with suitable characteristics for amplifying the source against the background. The image $y(\vec{x})$ is convolved with a filter $\psi(\vec{x})$:

$$\omega(\vec{x}) = \int y(\vec{u})\psi(\vec{x} - \vec{u}) d\vec{u} \quad (2)$$

The MF is defined as the linear filter that is an unbiased estimator of the source flux and minimizes the variance of the filtered map. In order to satisfy these mathematical constraints, if we assume that the beam is circularly symmetric and the background a homogeneous and isotropic random field, the MF must be defined in Fourier space as

$$\psi(q) = k \frac{\tau(q)}{P(q)} \quad (3)$$

where $\tau(q)$ is the Fourier transform of the beam, $P(q)$ the background power spectrum and k the normalization constant. With this definition, the MF gives the maximum amplification of the compact source with respect to the background. Once the source has been amplified, point sources are detected in the filtered map as peaks above a given threshold, typically 5σ , with σ the r.m.s deviation of the filtered map. The MF has been used both with simulations [28] and real data [29]. In this last paper, the WMAP team estimated the fluxes by fitting to a Gaussian profile plus a planar baseline. In [24] the MF was also applied to the detection of clusters. The use of wavelets for source detection is an interesting alternative to the MF. Wavelets are compensated linear filters, i.e their integral is zero, that help to remove the background contribution and yield a high source amplification. Since the beam is approximately Gaussian, the Mexican Hat Wavelet (MHW), constructed as the Laplacian of a Gaussian function, adapts itself very well to the detection problem. The MHW depends on the scale R , a parameter that determines the width of the wavelet:

$$\psi(q) \propto (qR)^2 \exp\left(-\frac{(qR)^2}{2}\right) \quad (4)$$

The MHW has been successfully applied to simulated CMB data [30]. The scale R is fixed in order to obtain the maximum amplification and the determination of the power spectrum is not necessary. A family of wavelets that generalize the MHW, the Mexican Hat Wavelet Family (MHWF) was presented in [31]. The performance of this family was compared with the MF in [28] and it produced similar results when implemented on Planck simulations. The MHWF was also applied to point source detection in WMAP images [32] by using a non-blind method. This method yielded a larger number of detections than the MF used by the WMAP group. The general expression of the MHWF is:

$$\psi(q) \propto (qR)^{2n} \exp\left(-\frac{(qR)^2}{2}\right) \quad (5)$$

n being a natural number. Further improvements can be obtained if we admit any real exponent such as in the Bi-parametric Adaptive Filter (BAF) [33].

The MF and the diverse types of wavelets do not use any prior information about the average number of sources in the surveyed patch, the flux distribution of the sources or other properties. Therefore, useful information is being neglected by these methods. In contrast, Bayesian methods provide a natural way to incorporate information about the statistical properties of both the source and the noise. Several Bayesian methods have been proposed in the literature for the detection problem [24, 34, 35]. These methods construct a posterior probability $Pr(\theta|D, H)$ by using Bayes' theorem

$$Pr(\theta|D, H) = \frac{Pr(D|\theta, H)Pr(\theta|H)}{Pr(D|H)} \quad (6)$$

where θ are the relevant parameters (positions, fluxes, sizes, etc.), D the data, and H the underlying hypothesis. In Bayesian terminology $Pr(D|\theta, H)$ is the likelihood, $Pr(\theta|H)$ is the prior and $Pr(D|H)$ is the Bayesian evidence. Different Bayesian techniques can differ in the priors or in the way of exploring the complicated posterior probability. PowellSnakes [34] is an interesting method, which has been applied with success to the compilation of the ERCSC for *Planck* frequencies between 30 and 143 GHz [15]. It uses Powell's minimization and physically motivated priors. This method can be also applied to cluster detection just by introducing a suitable prior on the cluster size.

A simple Bayesian way of determining the position of the sources and estimating their number and flux densities has been presented in [35]. Whereas by the MF, or by wavelets, sources are detected above an arbitrary threshold, Bayesian methods select them in a more natural way, for instance by comparing the posterior probability of two hypothesis: presence or absence of the source. In the next subsection we will explore multichannel methods that help improve the detection performance

3.2. Multi-channel detection

The flux density distribution, f_ν , of extragalactic radio sources as a function of frequency, ν , is usually approximated by a power law, although this approximation is only valid in

limited frequency intervals, i.e. $f_\nu \propto (\nu/\nu_0)^\alpha$, with ν_0 being some frequency of reference. Nevertheless, the so called “spectral index”, α , changes from source to source and this formula is not reliable when the range of frequencies is wide enough. In [36] a scheme for channel combination was proposed that makes the spectral behavior irrelevant. This method is called matrix multifilters (MTXFs) and relies on the application of a set ($N \times N$ matrix) of linear filters which combine the information of the N channels in such a way that: 1) an unbiased estimator of the source flux at each channel is obtained; and 2) the variance of the estimator is minimum. Note that the method does not mix the images in a single map, but it produces N maps in which the sources are conveniently amplified. The method defaults to the MF when there is no cross-correlation among the channels. When there is a non negligible correlation among the channels, as is the case for microwave images taken at different frequencies where CMB and Galactic foregrounds are present in all the images, this method gives a clear increase of the amplification when compared with the MF.

Now, we discuss a method tailored for cluster detection through the thermal SZ effect. Matched Multifilters (MMF) [37] combine N channels in a single image, incorporating the information about the spectral behavior (thermal SZ effect) and with the N filters depending on a scale parameter S . The filters are constructed in the usual way, by imposing unbiasedness and minimum variance. The MMF is given (in matrix notation) by

$$Y(q) = \alpha \mathbf{P}^{-1} F, \quad \alpha^{-1} = \int d\mathbf{q} F^t \mathbf{P}^{-1} F, \quad (7)$$

where F is the column vector $[f_\nu \tau_\nu]$, which incorporates the spectral behavior f_ν and the shape of the cluster at each frequency τ_ν and \mathbf{P} is the cross-power spectrum. Since the cluster size is not known a priori, the images are convolved with a set of filters with different scales S_i , and it has been proven that the amplification is maximum when the chosen scale coincides with the cluster size. A common pressure profile is assumed for the clusters. The detection is performed by searching for the maxima of the filtered map above a given threshold. The estimated amplitude of the thermal SZ effect is given by the amplitude at the maxima.

MMF can also be adapted to detect the fainter kinematic SZ effect. In this case an orthogonality condition with respect to the spectral behavior of the thermal SZ effect is imposed. Together with the usual unbiasedness and minimum variance conditions, this last constraint helps cancel out the thermal SZ effect contamination [38]. A MMF can also be designed for point source detection, by incorporating the (unknown) spectral behavior of the sources as a set of parameters in the filter, it has also been proven that the amplification is maximum when these parameters coincide with the real source spectrum. By changing the parameters and selecting those which give the maximum amplification, in [39] the authors were able to increase the number of point source detections in the WMAP 7-year maps.

Finally, a multi-channel Bayesian method has been developed recently, Powell-Snakes II [40]. This method constructs a posterior distribution by combining the likelihood and the prior information of the different channels. It is an extension of Powell-Snakes I and uses prior information on the positions, number of sources, intensities, sizes and spectral parameters. The method is suitable both for point sources and for clusters. It is worth noting that maximizing the likelihood when the sources are well separated, i.e. in the absence of source

blending, amounts to using the MMF presented above. Here we have briefly summarized the most important topics on the subject: a more detailed review can be found in [41].

4. Sunyaev-Zeldovich effect in clusters of galaxies

The Sunyaev-Zeldovich effect (SZ, [22]) accounts for the interaction between a hot plasma (in a cluster environment) and the photons of the CMB. When CMB photons cross a galaxy cluster, some of these photons interact with the free electrons in the hot plasma through inverse Compton scattering. The temperature change observed in a given direction, θ , and at the frequency ν , can be described as

$$\Delta T(\theta, \nu) = C_0 \int n_e(l) T(l) dl \quad (8)$$

where C_0 contains all the relevant constants including the frequency dependence ($g_x = x(e^x + 1)/(e^x - 1) - 4$, with $x = h\nu/kT$), n_e is the electron density and T is the electron temperature. The integral is performed along the line of sight.

The same electrons that interact with the CMB photons emit X-rays through the bremsstrahlung process:

$$S_x(\theta, \nu) = S_0 \frac{\int n_e^2 T^{1/2} dl}{D_\ell(z)^2} \quad (9)$$

where $D_\ell(z)$ is the luminosity distance. The quantity S_0 contains all the relevant constants and frequency dependence. Combining X-ray and SZ observations it is thus possible to reduce the degeneracy between different models due to their different dependency on T and especially with n_e .

Due to the nature of the microwave radiation, water vapour (and hence our atmosphere) presents a challenge for studying this radiation from the ground. Observations have to be carried out through several windows where the transmission of the microwave light is maximized. In recent years, ground-based experiments have benefited from important progress in the development of very sensitive bolometers. These bolometer arrays when combined with superb atmospheric conditions – found in places like the South Pole and the Atacama desert (with extremely low levels of water vapour) – have allowed, for the first time at all, galaxy clusters to be mapped in great detail through the SZ effect. The South Pole Telescope (or SPT; see, e.g., [42]) and the Atacama Cosmology Telescope (or ACT; see, e.g., [43]) are today the most important ground-based experiments carrying out these observations.

From space, the *Planck* satellite – even though it lacks the spatial resolution of ground-based experiments – complements them by applying a full-sky coverage, a wider frequency range and a better understanding of Galactic and extragalactic foregrounds. In particular, *Planck* is better suited than ground-based experiments to detect large angular scale SZ signals like nearby galaxy clusters or the diffuse SZ effect. In fact, ground-based experiments can have their large angular scales affected by atmospheric fluctuations that need to be removed, carefully. This removal process can distort the modes that include the large angular scales signal. On the contrary, *Planck* data does not suffer from these limitations

and its relatively poor angular resolution (if compared to some ground experiments) can be used to its advantage. The wide frequency coverage and extremely high sensitivity of *Planck* allows for detailed foreground (and CMB) removal that could overwhelm the weak signal of the SZ effect. *Planck* data will help improve the understanding of the distribution and the characteristics of the plasma in clusters. The conclusions derived on the internal structure of clusters will ultimately have an impact on other works that focus on deriving cosmological parameters. In fact, cosmological studies cannot by themselves disentangle among the uncertainties in the physics inside galaxy clusters.

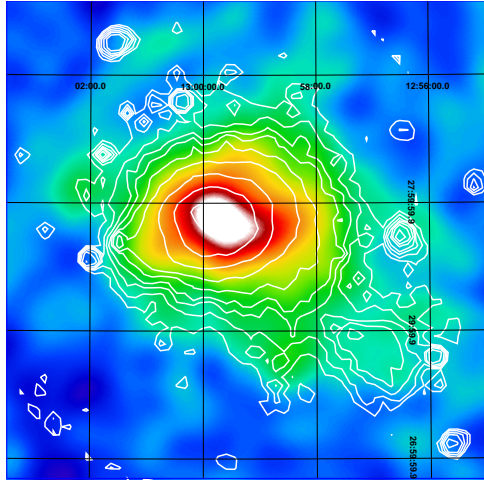


Figure 4. Fig. 1 from [44]. Coma cluster as seen by *Planck*. Contours show the the X-ray emission from Coma. Credit: *Planck* Collaboration, *A&A*, Vol. 536, A8, 2011, reproduced with permission © ESO.

The *Planck* satellite is currently detecting hundreds of clusters of galaxies through the thermal SZ effect. One of the peculiarities of the SZ effect is that the change in the CMB temperature in the direction of a cluster is independent of the distance to that cluster. This makes the SZ an ideal tool to explore the high redshift Universe. *Planck* is perfect for studying the most massive clusters in the Universe and is expected to see clusters beyond $z = 1$. Earlier results on galaxy clusters obtained by *Planck* have been presented in a subset of the *Planck* Early results papers and, more specifically, can be found in [44–49] and also in [50], where new results based on additional data are starting to be presented.

Among the first results published by the *Planck* collaboration on the SZ effect, the Coma cluster (see Fig. 4) constitutes one of the most spectacular ones. Coma is a nearby massive cluster that is well resolved by *Planck*. Fig. 4 shows the power of *Planck* to study the SZ effect with unprecedented quality. In the near future, studies based on *Planck* data alone or combined with X-ray data will reveal new details about the internal structure of this and other clusters.

Planck's earlier results include the detection of almost 200 clusters through their SZ signature ([44]). *Planck* is particularly sensitive to phenomena that increase the pressure, like mergers or superclusters. One such supercluster was detected by *Planck* [45]. Most of the clusters seen by *Planck* in the early analysis were known nearby objects but some of them were

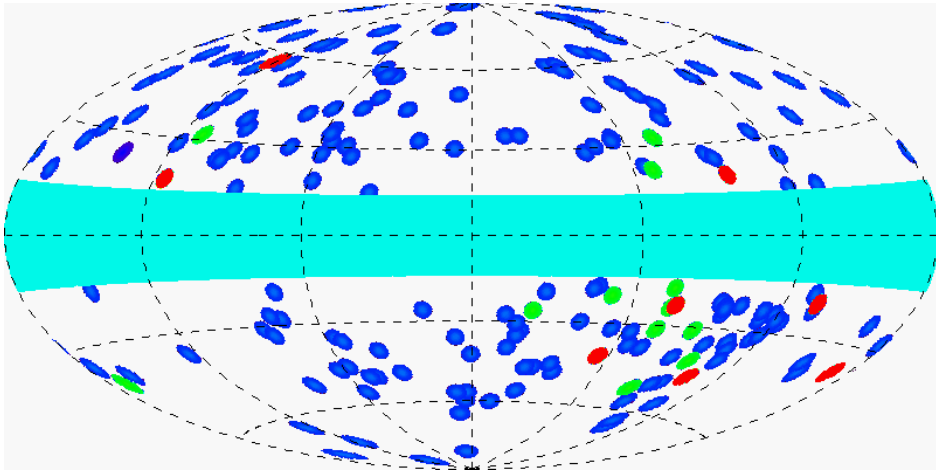


Figure 5. Fig. 3 from [44]. Distribution of *Planck* clusters that were already known (blue) and the new cluster candidates (green and red). Credit: *Planck* Collaboration, *A&A*, Vol. 536, A8, 2011, reproduced with permission © ESO.

new clusters, that have been later confirmed by X-ray and/or optical follow up. Fig. 5 shows the distribution in the sky of clusters of galaxies as seen by *Planck*. This includes the most massive clusters in the nearby and intermediate distance Universe. The redshift independence of the SZ effect can be appreciated in Fig. 6 (next page), which shows the relative flatness of the selection function of *Planck* as compared to cluster selections based on X-ray luminosity. New analysis based on better data will improve the selection function by reducing the limiting mass as a function of redshift. It is expected [5] that *Planck* will increase the number of known clusters in a significant way and, in particular, it will explore the high-redshift regime, detecting the most massive clusters at these high redshifts.

One of the most interesting conclusions derived by these earlier results comes from the combination of X-ray and SZ data. Earlier studies based on X-ray data were able to conclude that there exists a universal profile that accurately describes the gas pressure in galaxy clusters [51]. The newly discovered (by *Planck*) SZ clusters seem to follow well this profile but small deviations were observed when comparing the mean SZ profile with the average profile derived from X-ray observations. Fig. 7 summarizes one of the main results of the paper [45] where it can be appreciated how the average profile of the SZ observations (red thick line) flattens towards the cluster center ($R_{500} \ll 1$) when compared to the average of a sample of cool, core relaxed X-ray clusters (thick blue line). This fact suggests that the new clusters detected by *Planck* tend to be non-cool core, morphologically disturbed clusters. This would explain why these clusters were not found by previous X-ray surveys but *Planck*, that is sensitive to the total pressure rather than to the distribution of the gas, has no problem in finding them.

Many other relevant results can be found in the first series of papers from the *Planck* ERCSC, including studies of scaling relations between SZ quantities and optical or X-ray ones. More recently, a new analysis based on 2.5 full sky surveys has studied the relationship between the Compton parameter and weak lensing mass estimates [50]. As shown in Fig. 8, this work is very promising and could allow – in the near future – the use of the Compton parameter

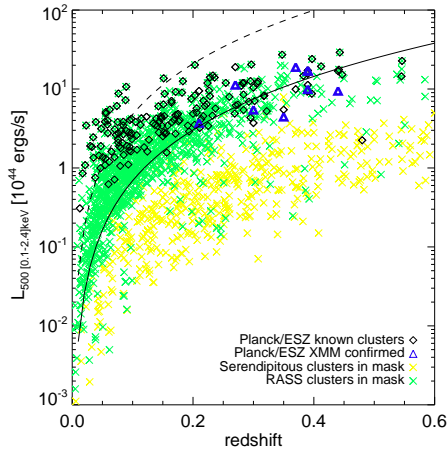


Figure 6. Fig. 21 from [44]. Redshift distribution as a function of luminosity for the 158 clusters from the Planck Early SZ sample (diamonds and triangles) identified with known X-ray clusters, compared with serendipitous and RASS clusters (crosses). See [44] for more details. Credit: *Planck* Collaboration, *A&A*, Vol. 536, A8, 2011, reproduced with permission © ESO.

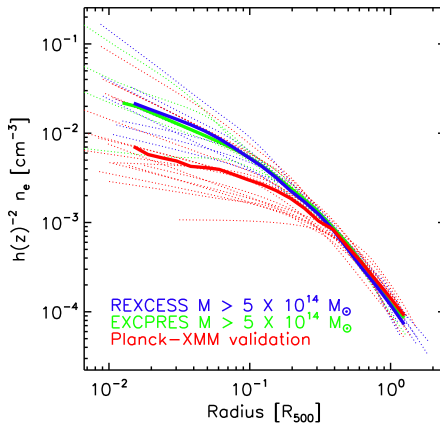


Figure 7. Fig. 10 from [45]. Scaled density profiles, derived from X-ray data, of the new *Planck* SZ clusters compared to those of similar mass systems from representative X-ray samples. Thick lines show the mean profile of each sample. Credit: *Planck* Collaboration, *A&A*, Vol. 536, A9, 2011, reproduced with permission © ESO.

as a mass proxy in cosmological studies, where a good mass estimator is crucial to derive accurate cosmological parameters from the analysis of a cluster sample.

After *Planck's* data release, science based on the SZ effect will change dramatically. *Planck* is expected to release more than 2 full sky surveys of data early in 2013, thus opening the door for multiple studies to be carried out by the scientific community. Cluster science based on the SZ effect will motivate many of these studies. Of particular interest will be those works that combine SZ effect and X-ray data. The different dependence of the SZ effect and X-ray emission with electron density and temperature allows for deprojection techniques

to reduce the uncertainties of the models. Also, the combination of X-ray and SZ data can be particularly powerful to study the clumpiness of the gas and deviations from spherical symmetry. An area where future *Planck* data will be used extensively will be the detection of new cluster candidates. The legacy *Planck* cluster catalogue will contain the most significant cluster signals. Hundreds of weaker SZ (and unknown) clusters will still be present in the public data but not in the legacy catalogue. Many groups will dig into the *Planck* data searching for these weaker signals. Among them there will be the most distant clusters at $z > 1$ that will be crucial for future cosmological studies.

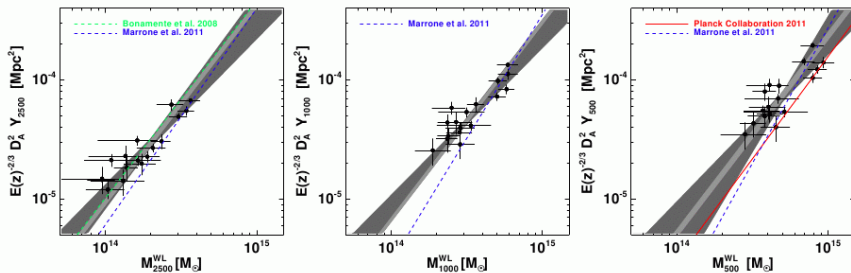


Figure 8. Fig. 1 from [50]. Correlation between the Compton parameter and the weak lensing mass. Credit: *Planck* Collaboration, A&A, submitted (ms AA/2012/19398), 2012, reproduced with permission © ESO.

Another area where *Planck* data might contribute significantly is in the study of energetic phenomena in galaxy clusters. The SZ effect is sensitive to the temperature of the Plasma (or more generally, to the speed distribution of the electrons). Hot clusters have an SZ spectrum that deviates from the standard shape. The shift (or relativistic correction) is more dramatic at higher frequencies ($\nu > 100$ GHz). Current X-ray missions like *Chandra* have some trouble determining the temperature of the plasma for clusters with high temperatures. On the contrary, the relativistic corrections to the SZ effect can dramatically boost the SZ signal in *Planck* at frequencies $\nu > 500$ GHz making, it easier to detect these clusters at these frequencies and also to derive constraints on the physical state of the plasma. A strong deviation in the spectrum could be an indication that very energetic phenomena (very high temperatures, shock waves, etc.) are operating on the cluster at large scales.

5. Extragalactic radio and far-IR sources

The *Planck* ERCSC [15] provides positions and flux densities of compact sources found in each of the nine *Planck* frequency maps. The flux densities are calculated using aperture photometry, with careful modeling of *Planck*'s elliptical beams⁸. These data on sources detected during the first 1.6 full-sky surveys offers, among other things, the opportunity of studying the statistical and emission properties of extragalactic radio and far-IR sources over a broad frequency range, never before fully explored by blind surveys.

⁸ Flux densities taken from the ERCSC should be divided by the appropriate colour correction to give the correct flux values for an assumed narrow band measurement at the central frequency.

As shown by [15], their Table 1, the full-sky surveys of the *Planck* satellite are – and will be, for years to come – unique in the millimetre, at $\lambda \leq 3$ mm, and submillimetre domains. The lack of data in this frequency range represented the largest remaining gap in our knowledge of bright extragalactic sources (i.e., normal and star-forming galaxies and Active Galactic Nuclei, AGNs) across the electromagnetic spectrum. In the course of its planned surveys, *Planck* has been able to measure the integrated flux of many hundreds of “radio” sources – i.e., sources at intermediate to high-redshift, dominated by synchrotron emission due to hot electrons in the inner jets of the Active Galactic Nucleus (AGN) of the source – and of many thousands “far-IR” sources – i.e., low-redshift dusty galaxies or sources with emission dominated by interstellar dust in thermal equilibrium with the radiation field – thus providing the *first complete full-sky catalogue* (ERCSC) of bright submillimetre sources. Thanks to this huge amount of new data it is thus possible to investigate the spectral energy distributions (SEDs) of EPS in a spectral domain very poorly explored before and, at the same time, their cosmological evolution, at least for some relevant source populations.

5.1. Synchrotron sources: “blazars”

The most recent estimates on source number counts of radio (synchrotron) sources up to $\sim 50 - 70$ GHz, and the optical identifications of the corresponding point sources (see, e.g., [52]), show that these counts are dominated by radio sources whose average spectral index is “flat”, i.e., $\alpha \simeq 0.0$ (with the usual convention $S_\nu \propto \nu^\alpha$). This result confirms that the underlying source population is essentially made of Flat Spectrum Radio Quasars (FSRQ) and BL Lac objects, collectively called “blazars”⁹, with minor contributions coming from other source populations [13, 54]. At frequencies > 100 GHz, however, there is now new information for sources with flux densities below about 1 Jy, coming from the South Pole Telescope (SPT) collaboration [55], with surveys over 87 deg^2 at 150 and 220 GHz, and from the Atacama Cosmology Telescope (ACT) survey over 455 deg^2 at 148 GHz [56].

The “flat” spectra of blazars are generally believed to result from the superposition of different components in the inner part of AGN relativistic jets, each with a different synchrotron self-absorption frequency [57]. At a given frequency, the observed flux density is thus dominated by the synchrotron-emitting component which becomes self-absorbed, and, in the equipartition regime, the resulting spectrum is approximately flat. Given their sensitivity and full sky coverage, *Planck* surveys are uniquely able to shed light on this transition from an almost “flat” to a “steep” regime in the spectra of blazar sources, which can be very informative on the ages of sources and on the inner jet processes which determine the acceleration of the electrons [58].

To study the spectral properties of the extragalactic radio sources in the *Planck* ERCSC [59] used a reference 30 GHz sample above an estimated completeness limit $S_{lim} \simeq 1.0$ Jy. Not all of these sources were detected at the $\geq 5\sigma$ level in each of the *Planck* frequency channels considered. Whenever a source was not detected in a given channel they replaced its (unknown) flux density by a 5σ upper limit, where for σ they used the average r.m.s.

⁹ Blazars are jet-dominated extragalactic objects characterized by a strongly variable and polarized emission of the non-thermal radiation, from low radio energies up to high energy gamma rays [53].

error estimated at each *Planck* frequency. Finally, for estimating spectral index distributions, these upper limits have been redistributed among the flux density bins by using a Survival Analysis technique and, more specifically, by adopting the Kaplan-Meyer estimator¹⁰[59].

In the sample analyzed by [59], the 30–100 GHz median spectral index is very close to the $\alpha \simeq -0.39$ found by [60] between 20 and 95 GHz, for a sample with 20 GHz flux density $S > 150$ mJy. Moreover, the 30–143 GHz median spectral index is in very good agreement with the one found by [56] for their bright ($S_\nu > 50$ mJy) 148 GHz-selected sample with complete cross-identifications from the Australia Telescope 20 GHz survey, i.e. $\alpha_{20}^{148} = -0.39 \pm 0.04$. Fig.9 presents the contour levels of the distribution of α_{70}^{143} vs. α_{30}^{70} (obtained using Survival Analysis) in the form of a 2D probability field: the colour scale can be interpreted as the probability of a given pair of spectral indices and a bending down, i.e. $\alpha < -0.5$, at high frequencies is displayed. In the whole, the results of [59] show that in their sample selected at 30 GHz a moderate steepening of spectral indices of EPS at high radio frequencies, i.e. $\gtrsim 70 - 100$ GHz, is clearly apparent¹¹.

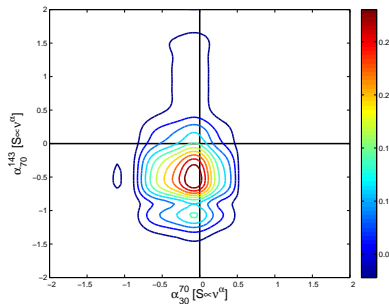


Figure 9. Fig. 7 from [59]. Contour levels of the distribution of α_{70}^{143} vs. α_{30}^{70} obtained by Survival Analysis, i.e., taking into account the upper limits to flux densities at each frequency. The colour scale can be interpreted as the probability of having any particular pair of values of the two spectral indices. The maximum probability corresponds to $\alpha_{30}^{70} \simeq -0.18$ and $\alpha_{70}^{143} \simeq -0.5$. Credit: Planck Collaboration, A&A, Vol. 536, A13, 2011, reproduced with permission © ESO.

As already noted, at high radio frequencies ($\nu > 30$ GHz) most of the bright extragalactic radio-sources are blazars. From the contour plot of Fig. 9 it is possible to see that the maximum probability of the spectral indices of blazars corresponds to $\alpha_{30}^{70} \simeq -0.18$ and $\alpha_{70}^{143} \simeq -0.5$. A secondary maximum can also be seen at $\alpha_{70}^{143} \simeq -1.2$. In a companion paper, i.e. [61], a detailed discussion on the modelling of the spectra of this source class is also presented. In this paper, spectral energy distributions (SEDs) and radio continuum spectra are presented for a northern sample of 104 extragalactic radio sources, based on the *Planck* ERCSC and simultaneous multifrequency data¹². The nine *Planck* frequencies, from 30 to 857 GHz, are complemented by a set of quasi-simultaneous observations ranging from radio to gamma-rays. SED modelling methods are discussed, with an emphasis on proper, physical

¹⁰ Since the fraction of upper limits is found to be always small (it reaches approximately 30% only in the less sensitive channel at 44GHz), the spectral index distributions are reliably reconstructed at each frequency.

¹¹ Some hints in this direction were previously found by other works on the subject. Additional evidence of spectral steepening is also presented in [61] by the analysis of a complete sample of blazars selected at 37GHz.

¹² The great amount of data present in the *Planck* ERCSC complemented with quasi-simultaneous ground-based observations at mm wavelengths have also enabled the study of the very interesting spectral properties of the rare peculiar and/or extreme radio sources detected by the *Planck* surveys [62].

modelling of the synchrotron bump using multiple components, and a thorough discussion on the original accelerated electron energy spectrum in blazar jets is presented. The main conclusion is that, at least for a fraction of the observed mm/sub-mm blazar spectra, the energy spectrum could be much harder than commonly thought, with a power-law index ~ 1.5 and the implications of this hard value are discussed for the acceleration mechanisms effective in blazar shocks.

It has also been shown by [59] that differential number counts at 30, 44, and 70 GHz are in good agreement with those derived from *WMAP* [29] data at nearby frequencies. The model proposed by [54] is consistent with the present counts at frequencies up to 70 GHz, but over-predicts the counts at higher frequencies by a factor of about 2.0 at 143 GHz and about 2.6 at 217 GHz¹³. As shown above, the analysis of the spectral index distribution over different frequency intervals, within the uniquely broad range covered by *Planck* in the mm and sub-mm domain, has highlighted an average *steepening* of source spectra above about 70 GHz. This steepening accounts for the discrepancy between the model predictions of [54] and the observed differential number counts at HFI frequencies.

In the fall of 2011, a successful explanation of the change detected in the spectral behavior of extragalactic radio sources (ERS) at frequencies above 70–80 GHz has been proposed by [63]. This paper makes a first attempt at constraining the most relevant physical parameters that characterize the emission of blazar sources by using the number counts and the spectral properties of extragalactic radio sources estimated from high-frequency radio surveys¹⁴. As noted before, a relevant steepening in blazar spectra with emerging spectral indices in the interval between -0.5 and -1.2 , is commonly observed at mm/sub-mm wavelengths. [63] interpreted this spectral behavior as caused, at least partially, by the transition from the optically-thick to the optically-thin regime in the observed synchrotron emission of AGN jets [64]. Indeed, a “break” in the synchrotron spectrum of blazars, above which the spectrum bends down, thus becoming “steep”, is predicted by models of synchrotron emission from inhomogeneous unresolved relativistic jets [65, 66]. Based on these models, [63] estimated the value of the frequency ν_M (and of the corresponding radius r_M) at which the break occurs on the basis of the flux densities of ERS measured at 5 GHz and of the most typical values for the relevant physical parameters of AGNs.

As displayed in Fig. 10, high frequency ($\nu \geq 100$ GHz) data on source number counts are the most powerful for distinguishing among different cosmological evolution models (see [63] for more details on the models plotted in Fig. 10)¹⁵. As clearly shown, these most recent data on number counts require spectral “breaks” in blazars’ spectra and clearly favor the

¹³ This implies that the contamination of the CMB APS by radio sources below the 1 Jy detection limit is lower than previously estimated. No significant changes are found, however, if we consider fainter source detection limits, i.e., 100 mJy, given the convergence between predicted and observed number counts.

¹⁴ The main goal of [63] was to present physically grounded models to extrapolate the number counts of ERS, observationally determined over very large flux density intervals at cm wavelengths down to mm wavelengths, where experiments aimed at accurately measuring CMB anisotropies are carried out.

¹⁵ The two most relevant models of [63], i.e. **C2Co** and **C2Ex**, assume different distributions of r_M – i.e., the smallest radius in the AGN jet from which optically-thin synchrotron emission can be observed – for BL Lacs and FSRQs, with the former objects that generate, in general, the synchrotron emission from more compact regions, implying higher values of ν_M (above 100 GHz for bright objects). These two models differ only in the r_M distributions for FSRQs: in the **C2Co** model the emitting regions are more compact, implying values of ν_M partially overlapping with those for BL Lacs, whereas in the **C2Ex** model they are more extended, thus predicting very different values of ν_M for FSRQs and BL Lacs.

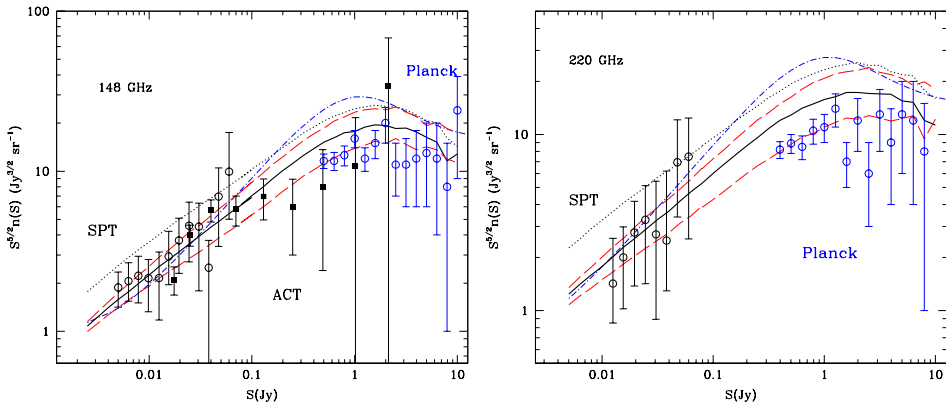


Figure 10. Comparison between predicted and observed differential number counts at 148 GHz (*left panel*) and at 220 GHz (*right panel*). Filled circles: ACT data; open black circles: SPT data; open blue circles: *Planck* ERCSC counts [59] at 143 GHz (*left panel*) and 217 GHz (*right panel*). The plotted lines indicate predictions of different models, as follows: **C0**(dotted lines), **C1** (thick continuous lines), **C2Ex** (lower red long-dashed lines) and **C2Co** (upper red long-dashed lines) and the [54] model (blue dash-dotted line). Credit: Tucci M., et al., *A&A*, Vol. 533, A57, 2011, reproduced with permission © ESO.

model **C2Ex**. According to this, most of the FSRQs (which are the dominant population at low frequencies and at Jy flux densities), differently from BL Lacs, should bend their flat spectrum before or around 100 GHz. The **C2Ex** model also predicts a substantial increase of the BL Lac fraction at high frequencies and bright flux densities¹⁶. On the whole, the results of [63] imply that the parameter r_M should be of parsec-scales, at least for FSRQs, in agreement with the theoretical predictions of [67], whereas values of $r_M \ll 1$ pc should be only typical of BL Lac objects or of rare, and compact, quasar sources.

5.2. Far-IR sources: Local dusty galaxies

The full-sky coverage of the *Planck* ERCSC provides an unsurpassed survey of galaxies at submillimetre (submm) wavelengths, representing a major improvement in the numbers of galaxies detected, as well as the range of far-IR/submm wavelengths over which they have been observed. The analysis done by [68] presented the first results on the properties of nearby galaxies using these data. They matched the ERCSC catalogue to IRAS-detected galaxies in the Imperial IRAS Faint Source Redshift Catalogue (IIFSCz) [69], so that they could measure the SEDs of these objects from 60 to 850 μm . This produced a list of 1717 galaxies with reliable associations between *Planck* and IRAS, from which they selected a subset of 468 for SED studies, namely those with strong detections in the three highest frequency *Planck* bands and no evidence of cirrus contamination. This selection has thus provided a first *Planck* sample of local, i.e. at redshift < 0.1 , dusty galaxies, very important for determining their emission properties and, in particular, the presence of different dust components contributing to their submm SEDs. Moreover, the richness of data on

¹⁶ This is indeed observed: a clear dichotomy between FSRQs and BL Lac objects has been found in the *Planck* ERCSC. Almost all radio sources show very flat spectral indices at LFI frequencies, i.e. $\alpha_{LFI} \geq -0.2$, whereas at HFI frequencies, BL Lacs keep flat spectra, i.e. $\alpha_{HFI} \geq -0.5$, with a high fraction of FSRQs showing steeper spectra, i.e. $\alpha_{HFI} \leq -0.5$.

extragalactic point sources gathered by *Planck* has allowed the measurement of the submm number density of bright ($S > 0.5 - 2$ Jy) dusty galaxies (and of synchrotron-dominated sources) for the first time.

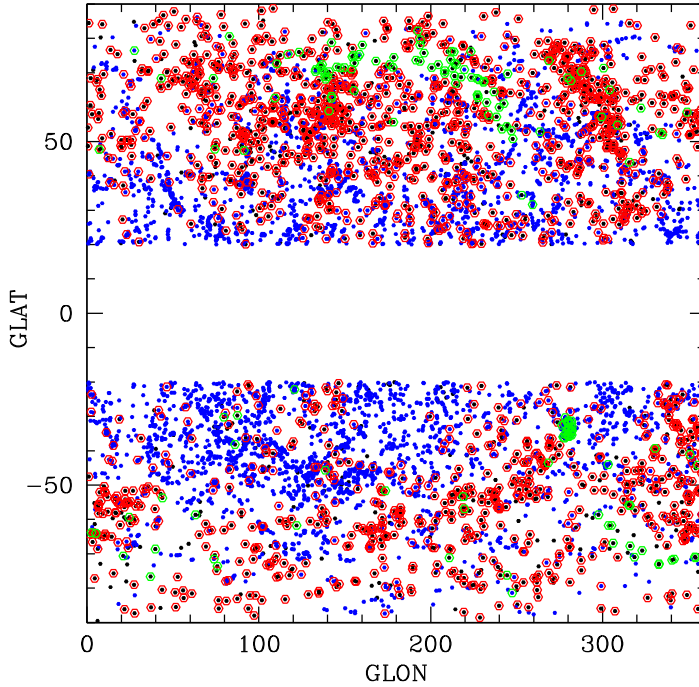


Figure 11. Fig. 2 from [68]. Sky plot of ERCSC sources in Galactic coordinates. ERCSC point-sources (black filled hexagons) and ERCSC sources flagged as extended (blue filled hexagons) are shown. Red hexagons are sources associated with IIFSCz IRAS FSC galaxies. Green hexagons are ERCSC sources not associated with IIFSCz, but associated with bright galaxies in NED (only for $|b| > 60^\circ$ for extended sources). Credit: Planck Collaboration, A&A, Vol. 536, A16, 2011, reproduced with permission © ESO.

Fig. 11 shows the sky distribution of ERCSC sources at $|b| > 20^\circ$, with sources flagged as extended in the ERCSC shown as blue filled hexagons, and point-sources shown in black. Associations with the IIFSCz are shown as red circles. The extended sources not associated with IIFSCz sources have a strikingly clustered distribution, which matches the areas of our Galaxy with strong cirrus emission, as evidenced by IRAS $100 \mu\text{m}$ maps. Therefore, the majority of these are cirrus sources and not extragalactic (see [68] for more details).

The studies of nearby galaxies detected by *Planck* [68] confirm the presence of cold dust in local galaxies and also largely in dwarf galaxies. The SEDs are fitted using parametric dust models to determine the range of dust temperatures and emissivities. They found evidence for colder dust than has previously been found in external galaxies, with temperatures $T < 20$ K. Such cold temperatures are found by using both the standard single temperature dust model with variable emissivity β , or a two dust temperature model with β fixed at 2. In

[68] it is also found that some local galaxies are both luminous and cool, with properties similar to those of the distant submm galaxies uncovered in deep surveys. This suggests that previous studies of dust in local galaxies have been biased away from such luminous cool objects. In most galaxies the dust SEDs are found to be better described by parametric models containing two dust components, one warm and one cold, with the cold component reaching temperatures as low as 10 K¹⁷. The main conclusion of [68] is that cold ($T < 20$ K) dust is thus a significant and largely unexplored component of many nearby galaxies. Furthermore, a new population of cool submm galaxies is detected, with presence of very cold dust ($T = 10 - 13$ K) showing a more extended spatial distribution than generally assumed for the gas and dust in galaxies.

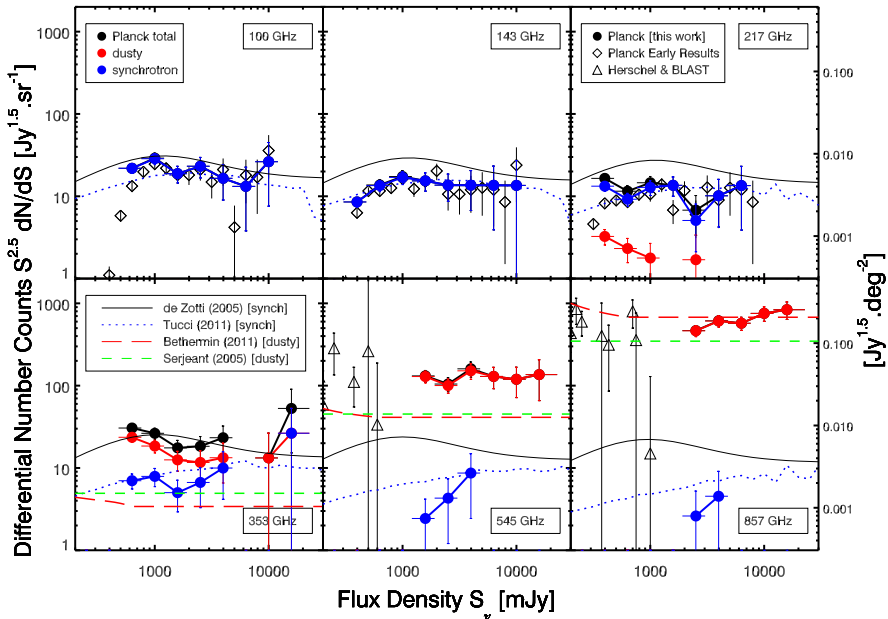


Figure 12. Fig. 9 from [70]. *Planck* differential number counts, normalized to the Euclidean value (i.e. $S^{2.5}dN/dS$), compared with models and other data sets. *Planck* counts: total (black filled circles); dusty (red circles); synchrotron (blue circles). Four models are also plotted: [54], dealing only with synchrotron sources – solid line; [63] dealing only with synchrotron sources – dots; [71] dealing only with dusty sources – long dashes; [72] dealing only with local dusty sources – short dashes. Other data sets: *Planck* early counts for 30 GHz-selected radio galaxies [59] at 100, 143 and 217 GHz (open diamonds); *Herschel* ATLAS and HerMES counts at 350 and 500 μm from [73] and [74]; BLAST at the same two wavelengths, from [75], all shown as triangles. Left vertical axes are in units of $\text{Jy}^{1.5} \text{sr}^{-1}$, and the right vertical axis in $\text{Jy}^{1.5} \text{deg}^{-2}$. Credit: Planck Collaboration, A&A, submitted (ms AA/2012/20053), 2012, reproduced with permission © ESO.

Very recently, using EPS samples selected from the first *Planck* 1.6 full-sky surveys, i.e. from the *Planck* ERCSC, [70] have derived number counts of extragalactic sources from 100 to 857 GHz (3 mm to 350 μm). Three zones (deep, medium and shallow) of approximately

¹⁷ Fits to SEDs of selected objects using more sophisticated templates derived from radiative transfer models confirm the presence of the colder dust found through parametric fitting.

homogeneous coverage are used to ensure a clean completeness correction¹⁸. For the first time, bright number counts of EPS at 353, 545 and 857 GHz (i.e., 850, 550 and 350 μm) have been calculated¹⁹. *Planck* number counts are found to be in the Euclidean regime in this frequency range, since the ERCSC comprises only bright sources ($S > 0.3$ Jy). The estimated number counts appear generally in agreement with other data sets, when available (see [70] for more details).

Using multi-frequency information to classify the sources as dusty- or synchrotron-dominated (and measure their spectral indices), the most striking result of [70] is the estimated contribution to the number counts by each population. These new estimates of number counts of synchrotron and of dust-dominated EPS (displayed in Fig. 12) have allowed new constraints to be placed on models which extend their predictions to bright flux densities, i.e. $S > 1$ Jy. A very relevant result is that the model **C2Ex** of [63] (see Section 5.1) is performing particularly well at reproducing the number counts of synchrotron-dominated sources up to 545 GHz. On the contrary, [70] highlights the failure of many models for number count predictions of dusty sources to reproduce all the high-frequency counts. The model of [71] agrees marginally at 857 GHz but is too low at 545 GHz and also at lower frequencies, whereas the model of [72] is marginally lower at 857 GHz, fits the data well at 545 GHz, but is too low at 353 GHz. The likely origin of the discrepancies is an inaccurate description of the galaxy SEDs used at low redshift in these models. Indeed a cold dust component, detected by [68], is rarely included in the models of galaxy SEDs at low redshift. On the whole, these results already obtained by the exploitation of the *Planck* ERCSC data are providing valuable information about the ubiquity of cold dust in the local Universe, at least in statistical terms, and are guiding to a better understanding of the cosmological evolution of EPS at mm/sub-mm wavelengths.

6. Cosmic Infrared Background anisotropies

The Cosmic Infrared Background (CIB) is the relic emission, at wavelengths larger than a few microns, of the formation and evolution of the galaxies of all types, including AGNs and star-forming systems [76–78]²⁰. The CIB accounts for roughly half of the total energy in the optical/infrared Extragalactic Background Light (EBL) [77], although with some uncertainty, and its SED peaks near 150 μm . Since local galaxies give rise to an integrated infrared output that amounts to only about a third of the optical one [79], there must have been a strong evolution of galaxy properties towards enhanced far-IR output in the past. Therefore, the CIB, made up by high density, faint and distant galaxies²¹ is barely resolved into its constituents. Indeed, less than 10% of the CIB is resolved by the *Spitzer* satellite at 160 μm

¹⁸ The sample, prior to the 80 % completeness cut, contains between 217 sources at 100 GHz and 1058 sources at 857 GHz over about 12,800 to 16,550 deg^2 (31 to 40 % of the sky). After the 80 % completeness cut, between 122 and 452 sources remain, with flux densities above 0.3 and 1.9 Jy, at 100 and 857 GHz, respectively.

¹⁹ More specifically, number counts have been provided of synchrotron-dominated sources at high frequency (353 to 857 GHz) and of dusty-dominated galaxies at lower frequencies (217 and 353 GHz).

²⁰ An important goal of studies of galaxy formation has thus been the characterization of the statistical behavior of galaxies responsible for the CIB - such as the number counts, redshift distribution, mean SED, luminosity function, clustering - and their physical properties, such as the roles of star-forming vs. accreting systems, the density of star formation, and the number density of very hot stars

²¹ The CIB records much of the radiant energy released by processes of structure formation occurred since the last scattering epoch, four hundred thousand years after the Big Bang, when the CMB was produced.

[75], about 10% by *Herschel* at $350\ \mu\text{m}$ [73]. Thus, in the absence of foreground (Galactic dust) and CMB emissions, and when the instrument noise is subdominant, maps of the diffuse emission at the angular resolution probed by the current surveys reveal a web of structures, characteristic of CIB anisotropies. With the advent of large area far-IR to millimeter surveys (*Herschel*, *Planck*, SPT, and ACT), CIB anisotropies thus constitute a new tool for structure formation and evolution studies.

CIB anisotropies are expected to trace large-scale structures and probe the clustering properties of galaxies, which in turn are linked to those of their hosting dark matter halos. Because the clustering of dark matter is well understood, observations of anisotropies in the CIB constrain the relationship between dusty, star-forming galaxies at high redshift, i.e. $z \geq 2$, and the underlying dark matter distribution. The angular power spectrum of CIB anisotropies has two contributions, a white-noise component caused by shot noise and an additional component caused by spatial correlations between the sources of the CIB. Correlated CIB anisotropies have already been measured by many space-borne as well as ground-based experiments (see [80] for more details). Depending on the frequency, the angular resolution and size of the survey, these measurements can probe two different clustering regimes. On small angular scales ($\ell \geq 2000$), they measure the clustering within a single dark matter halo and, accordingly, the physics governing how dusty, star-forming galaxies form within a halo. On large angular scales, i.e. $200 \leq \ell \leq 2000$, CIB anisotropies measure clustering between galaxies in different dark matter halos. These measurements primarily constrain the large-scale, linear bias, b , of dusty galaxies, which is usually assumed to be scale-independent over the relevant range.

Thanks to the exceptional quality of the *Planck* data, [80] were able to measure the clustering of dusty, star-forming galaxies at 217, 353, 545, and 857 GHz with unprecedented precision. The CIB maps were cleaned using templates: HI for Galactic cirrus; and the *Planck* 143 GHz maps for CMB. Having HI data is necessary to cleanly separate CIB and cirrus fluctuations. After careful cleaning, they obtained CIB anisotropy maps that reveal structures produced by the cumulative emission of high-redshift, dusty, star-forming galaxies. The maps are highly correlated at high *Planck* frequencies, whereas they decorrelate at lower *Planck* HFI frequencies. [80] then computed the power spectra of the maps and their associated errors using a dedicated pipeline and ended up with measurements of the APS of the CIB anisotropy, C_ℓ , at 217, 353, 545, and 857 GHz, with high signal-to-noise ratio over the range $200 < \ell < 2000$. These measurements compare very well with previous measurements at higher ℓ ²².

Moreover, from *Planck* data alone [80] could exclude a model where galaxies trace the (linear theory) matter power spectrum with a scale-independent bias: that model requires an *unrealistic* high level of shot noise to match the small-scale power they observed. Consequently, an alternative model that couples the dusty galaxy, parametric evolution model of [71] with a halo model approach has been developed (see [80], again, for more details). Characterized by only two parameters, this model provides an excellent fit to our measured anisotropy angular power spectrum for each frequency treated independently. In the near future, modelling and interpretation of the CIB anisotropy will be aided by the use

²² The SED of CIB anisotropies is not different from the CIB mean SED, even at 217 GHz. This is expected from the model of [71] and reflects the fact that the CIB intensity and anisotropies are produced by the same population of sources.

of cross-power spectra between bands, and by the combination of the *Planck* and *Herschel* data at 857 and 545/600 GHz and *Planck* and SPT/ACT data at 220 GHz.

7. Acknowledgements

LT, FA and JMD acknowledge partial financial support from the Spanish Ministry of Science and Innovation (MICINN) under project AYA2010-21766-C03-01. CB acknowledges partial financial support by ASI through ASI/INAF Agreement I/072/09/0 for the Planck LFI Activity of Phase E2 and by MIUR through PRIN 2009 grant n. 2009XZ54H2. The analysis of the *Planck* full-sky maps has been performed by means of the HEALPix package [12]. We thank the Editorial Board of Astronomy and Astrophysics (European Southern Observatory; ESO) for having granted us the permission to reproduce many Figures originally published in (or submitted to) the same Journal. Credits are indicated in each one of the Figures we used. Many thanks are due to Douglas Scott, for carefully reading the original manuscript and for his very useful suggestions. We also warmly thank the *Planck* Collaboration and, in particular, all the members of the *Planck* Working Groups 2, 5 and 6 and of the LFI Core Team A09, with whom we shared the analysis and the interpretation of *Planck* data as for the subject here discussed, i.e. "extragalactic compact sources". Finally, we also thank the members of the *Planck* Science Team (ST) and of the *Planck* Editorial Board (EB) for granting us the permission of publishing this Chapter.

Author details

Luigi Toffolatti^{1,2,*}, Carlo Burigana^{3,4},
Francisco Argüeso^{2,5} and José M. Diego²

* Address all correspondence to: ltoffolatti@uniovi.es

1 Department of Physics, University of Oviedo, Oviedo, Spain

2 IFCA-CSIC, University of Cantabria, Santander, Spain

3 National Institute of Astrophysics - Institute of Space Astrophysics and Cosmic Physics (INAF-IASF), Bologna, Italy

4 Department of Physics, University of Ferrara, Ferrara, Italy

5 Department of Mathematics, University of Oviedo, Oviedo, Spain

References

- [1] Tauber J.A., Mandolesi N., Puget J.-L., et al. (2010) Planck pre-launch status: the Planck mission. *Astronomy and Astrophysics*, 520, A1:1-22.
- [2] Planck Collaboration I. (2011) Planck early results. I. The Planck Mission. *Astronomy and Astrophysics*, Vol. 536, A1:1-16.
- [3] Planck HFI Core Team (2011a). Planck early results. IV. First assessment of the High Frequency Instrument in-flight performance. *Astronomy and Astrophysics*, Vol. 536, A4:1-20.

- [4] Mennella A., Butler C., Curto A., et al. (2011). Planck early results. III. First assessment of the Low Frequency Instrument in-flight performance. *Astronomy and Astrophysics*, Vol. 536, A3:1-29.
- [5] *Planck* Collaboration, 2005, ESA Science Report, ESA-SCI(2005)/01, arXiv:0604069.
- [6] N. Mandolesi, et al., (2010) Planck pre-launch status: The Planck-LFI programme *Astronomy and Astrophysics*, Vol. 520, A3:1-24.
- [7] J.-M. Lamarre, et al., (2010) Planck pre-launch status: The HFI instrument, from specification to actual performance. *Astronomy and Astrophysics*, Vol. 520, A9:1-20.
- [8] P. Giommi, et al., (2012) Simultaneous Planck, Swift, and Fermi observations of X-ray and γ -ray selected blazars. *Astronomy and Astrophysics*, Vol. 541, A160:1-59.
- [9] Knox, L. (1995) Determination of inflationary observables by cosmic microwave background anisotropy experiments. *Physical Review D*, Vol. 52:4307-4318.
- [10] Planck HFI Core Team (2011b). Planck early results. VI. The High Frequency Instrument data processing. *Astronomy and Astrophysics*, Vol. 536, A6:1-47.
- [11] Zacchei A., Maino D., Baccigalupi C., et al. (2011) Planck early results. V. The Low Frequency Instrument data processing. *Astronomy and Astrophysics*, Vol. 536, A5:1-19.
- [12] K.M. Górski, et al. (2005) HEALPix: A Framework for High-Resolution Discretization and Fast Analysis of Data Distributed on the Sphere. *The Astrophysical Journal*, Vol. 622, 759-780.
- [13] Toffolatti L., Argüeso F., De Zotti G., et al. (1998) Extragalactic source counts and contributions to the anisotropies of the cosmic microwave background: predictions for the Planck Surveyor mission. *Monthly Notices of the Royal Astronomical Society*, 297:117-127.
- [14] Tucci M., and Toffolatti L. (2012) The impact of polarized extragalactic radio sources on the detection of CMB anisotropies in polarization. *Advances in Astronomy*, Special Issue: "Astrophysical Foregrounds in Microwave Surveys", Hindawi Publ. Co., Editor: C. Burigana, Vol. 2012, Article ID 624987:1-17 (doi:10.1155/2012/624987).
- [15] Planck Collaboration VII. (2011) Planck Early results. VII. The Planck Early Release Compact Source Catalogue. *Astronomy and Astrophysics*, Vol. 536, A7:1-26.
- [16] Komatsu E., et al. (2010) Non-Gaussianity as a Probe of the Physics of the Primordial Universe and the Astrophysics of the Low Redshift Universe. *Astro2010: The Astronomy and Astrophysics Decadal Survey*, Science White Papers, Vol. 158.
- [17] Bartolo N., Komatsu E., Matarrese S., and Riotto A. (2010) Non-Gaussianity from inflation: Theory and observations. *Physics Report*, Vol. 402:103-114.

- [18] Verde L., Wang L.M., Heavens A., and Kamionkowski M. (2000) Large-scale structure, the cosmic microwave background, and primordial non-gaussianity. *Monthly Notices of the Royal Astronomical Society*, Vol. 313:L141-L145.
- [19] Komatsu E., and Spergel D.N. (2001) Acoustic signatures in the primary microwave background bispectrum, *Physical Rev. D*, Vol. 63:063002
- [20] Babich D., Creminelli P., and Zaldarriaga M. (2004) The shape of non-Gaussianities, *Journal of Cosmology and Astroparticle Physics*, Vol. 08:009-018.
- [21] Xia J.Q., Baccigalupi C., Matarrese S., Verde L., Viel M. (2011) Constraints on primordial non-Gaussianity from large scale structure probes. *Journal of Cosmology and Astroparticle Physics*, Vol. 08:033 (JCAP08(2011)033).
- [22] Sunyaev, R., Zeldovich, Ya.B. (1972) The Observations of Relic Radiation as a Test of the Nature of X-Ray Radiation from the Clusters of Galaxies. *Comments on Astrophysics and Space Physics* 4:173-179.
- [23] Herranz D., Sanz J.L., Barreiro R., Martínez-González E. (2002) Scale-adaptive Filters for the Detection/Separation of Compact Sources. *The Astrophysical Journal* 580:610-625.
- [24] Schulz A. E., White M. (2003) Survey of Galaxy Clusters with the Sunyaev-Zeldovich Effect. *The Astrophysical Journal* 586:723-730.
- [25] Hobson M., McLachlan C. (2003) A Bayesian Approach to Discrete Object Detection in Astronomical Data Sets. *Monthly Notices of The Royal Astronomical Society* 338:765-784.
- [26] Bertin E., Arnouts S. (1996) SExtractor: Software for Source Extraction. *Astronomy and Astrophysics Supplement* 117:393-404.
- [27] Tegmark M., de Oliveira-Costa A. (1998) Removing Point Sources from Cosmic Microwave Background Maps. *The Astrophysical Journal Letters* 500:L83-L86.
- [28] López-Caniego et al. (2006) Comparison of Filters for the Detection of Point Sources in Planck Simulations. *Monthly Notices of The Royal Astronomical Society*, Vol. 370:2047-2063.
- [29] Wright E. L. et al. (2009) Five-year Wilkinson Anisotropy Probe Observations: Source Catalog. *The Astrophysical Journal Supplement Series*, Vol. 180:283-295.
- [30] Cayón L. et al. (2000) Isotropic Wavelets. A Powerful Tool to Extract Point Sources from Cosmic Microwave Background Maps. *Monthly Notices of The Royal Astronomical Society*, Vol. 315:757-761.
- [31] González-Nuevo et al. (2006) The Mexican Hat Wavelet Family: Application to Point-Source Detection in Cosmic Microwave Background Maps. *Monthly Notices of The Royal Astronomical Society* 369:1603-1610.

- [32] López-Caniego et al. (2007) Non-blind Catalogue of Extragalactic Sources from the Wilkinson Microwave Anisotropy Probe (WMAP) first 3-year survey data. *The Astrophysical Journal Supplement Series* 170:108-125.
- [33] López-Caniego M., Vielva P. (2012) Biparametric Adaptive Filter: Detection of Compact Sources in Complex Microwave Backgrounds. *Monthly Notices of The Royal Astronomical Society*, Vol. 421:2139-2154.
- [34] Carvalho P., Rocha G., Hobson M. (2009) A Fast Bayesian Approach to Discrete Object Detection in Astronomical Data Sets. *Monthly Notices of The Royal Astronomical Society* 393:681-702.
- [35] Argüeso F. et al. (2011) A Bayesian Technique for the Detection of Point Sources in CMB Maps. *Monthly Notices of The Royal Astronomical Society* 414:410-417.
- [36] Herranz D., Sanz J.L. (2008) Matrix Filters for the Detection of Extragalactic Point Sources in Cosmic Microwave Background Images. *IEEE Journal on Selected Topics in Signal Processing* 2:727-734.
- [37] Herranz D., et al. (2002) Filtering Techniques for the Detection of Sunyaev-Zeldovich Clusters in Multifrequency Maps. *Monthly Notices of The Royal Astronomical Society* 336:1057-1068.
- [38] Herranz D., Sanz J. L., Barreiro R., López-Caniego M. (2005) The Estimation of the Sunyaev-Zeldovich Effects with Unbiased Multifilters. *Monthly Notices of The Royal Astronomical Society* 356:944-954.
- [39] Lanz L.F., et al. (2012) Extragalactic Point Source Detection in WMAP 7-year Data at 61 and 94 GHz. *Monthly Notices of The Royal Astronomical Society*, submitted. ArXiv:astro/ph:1110.6877.
- [40] Carvalho P., Rocha G., Hobson M., Lasenby A. (2012) PowellSnakes II: A Fast Bayesian Approach to Discrete Object Detection in Multi-frequency Astronomical Data Sets. *Monthly Notices of The Royal Astronomical Society*, submitted. ArXiv:astro/ph:1112.4933.
- [41] Herranz D., Argüeso F., Carvalho P. (2012) Compact Sources Detection in Multichannel Microwave Surveys: From SZ Clusters to Polarized Sources. *Advances in Astronomy*, 2012:1-14. doi:10.1155/2012/410965.
- [42] Hall N.R., Keisler R., Knox L., et al. (2010) Angular Power Spectra of the Millimeter-wavelength Background Light from Dusty Star-forming Galaxies with the South Pole Telescope. *The Astrophysical Journal*, Vol. 718:632-646.
- [43] Fowler J.W., Acquaviva V., Ade P.A.R., et al. (2010) The Atacama Cosmology Telescope: A Measurement of the $600 < \ell < 8000$ Cosmic Microwave Background Power Spectrum at 148 GHz. *The Astrophysical Journal*, Vol. 722:1148-1161.
- [44] Planck Collaboration VIII. (2011) Planck Early results. VIII. The all-sky early Sunyaev-Zeldovich cluster sample. *Astronomy and Astrophysics*, Vol 536, A8:1-28.

- [45] Planck Collaboration IX. (2011) Planck Early results. VIII. XMM-Newton follow-up for validation of Planck cluster candidates. *Astronomy and Astrophysics*, Vol 536, A9:1-20.
- [46] Planck Collaboration X. (2011) Planck Early results. X. Statistical analysis of Sunyaev-Zeldovich scaling relations for X-ray galaxy clusters. *Astronomy and Astrophysics*, Vol 536, A10:1-14.
- [47] Planck Collaboration XI. (2011) Planck Early results. XI. Calibration of the local galaxy clusters Sunyaev-Zeldovich scaling relations. *Astronomy and Astrophysics*, Vol 536, A11:1-14.
- [48] Planck Collaboration XII. (2011) Planck Early results. XII. Cluster Sunyaev-Zeldovich optical scaling relations. *Astronomy and Astrophysics*, Vol 536, A12:1-10.
- [49] Planck Collaboration XXVI. (2011) Planck Early results. XXVI. Detection with Planck and confirmation by XMM-Newton of PLCK G266.6-27.3, an exceptionally X-ray luminous and massive galaxy cluster at $z \sim 1$. *Astronomy and Astrophysics*, Vol 536, A26:1-7.
- [50] Planck Collaboration III. (2012) Planck Intermediate results. III. The relation between galaxy cluster mass and Sunyaev-Zeldovich signal. *Astronomy and Astrophysics*, submitted. [arXiv.org//1204.2743v1](https://arxiv.org/abs/1204.2743v1).
- [51] Arnaud M., Pratt G.W., Piffaretti R., Böhringer H., Croston J.H., Pointecouteau E. (2010) The universal galaxy cluster pressure profile from a representative sample of nearby systems (REXCESS) and the $Y_{SZ} - M_{500}$ relation. *Astronomy and Astrophysics*, Vol 517, A92:1-20.
- [52] Massardi M., Ekers R.D., Murphy T., et al. (2008) The Australia Telescope 20-GHz (AT20G) Survey: the Bright Source Sample. *Monthly Notices of the Royal Astronomical Society*, 384:775-802.
- [53] Urry C.M., Padovani P. (1995) Unified Schemes for Radio-Loud Active Galactic Nuclei. *Publication of the Astronomical Society of the Pacific*, 107:803-860.
- [54] De Zotti G., Ricci R., Mesa D., et al. (2005) Predictions for high-frequency radio surveys of extragalactic sources. *Astronomy and Astrophysics*, Vol. 431:893-903.
- [55] Vieira J., Crawford T.M., Switzer E.R., et al. (2010) Extragalactic Millimeter-wave Sources in South Pole Telescope Survey Data: Source Counts, Catalog, and Statistics for an 87 Square-degree Field. *The Astrophysical Journal*, Vol. 719:763-783.
- [56] Marriage T.A., Juin J.B., Lin Y., et al. (2011) Atacama Cosmology Telescope: Extragalactic Sources at 148 GHz in the 2008 Survey. *The Astrophysical Journal*, Vol. 731, A100:1-15.
- [57] Kellermann K.I., and Pauliny-Toth I.I.K. (1969) The Spectra of Opaque Radio Sources. *The Astrophysical Journal Letters*, 155:L71-L75.

- [58] Marscher A. (1980) Relativistic jets and the continuum emission in QSOs. *The Astrophysical Journal*, 235:386-391.
- [59] Planck Collaboration XIII. (2011) Planck early results. XIII. Statistical properties of extragalactic radio sources in the Planck Early Release Compact Source Catalogue. *Astronomy and Astrophysics*, Vol 536, A13:1-10.
- [60] Sadler E., Ricci R., Ekers R., et al. (2008) The extragalactic radio-source population at 95GHz. *Monthly Notices of the Royal Astronomical Society*, 385:1656-1672.
- [61] Planck Collaboration XV. (2011) Planck early results. XV. Spectral energy distributions and radio continuum spectra of northern extragalactic radio sources. *Astronomy and Astrophysics*, Vol. 536, A15:1-56.
- [62] Planck Collaboration XIV. (2011) Planck early results. XIV. ERCSC validation and extreme radio sources. *Astronomy and Astrophysics*, Vol. 536, A14:1-18.
- [63] Tucci M., Toffolatti L., De Zotti G., and Martínez-González E. (2011). High-frequency predictions for number counts and spectral properties of extragalactic radio sources. New evidence of a break at mm wavelengths in spectra of bright blazar sources. *Astronomy and Astrophysics*, Vol. 533, A57:1-21.
- [64] Marscher A.P. (1996) The Inner Jets of Blazars. Published in "Energy transport in radio galaxies and quasars", A.S.P. Conf. Series, eds. P.E. Hardee, A.H. Bridle and J.A. Zensus (San Francisco: Astronomical Society of the Pacific), Vol. 100:45-54.
- [65] Blandford R., and Königl A. (1979) Relativistic jets as compact radio sources. *The Astrophysical Journal*, Vol. 232:34-48.
- [66] Königl A. (1981) Relativistic jets as X-ray and gamma-ray sources. *The Astrophysical Journal*, Vol. 243:700-709.
- [67] Marscher A.P., Gear W.K. (1985) Models for high-frequency radio outbursts in extragalactic sources, with application to the early 1983 millimeter-to-infrared flare of 3C 273. *The Astrophysical Journal*, Vol. 298:114-127.
- [68] Planck Collaboration XVI. (2011) Planck early results. XVI. The Planck view of nearby galaxies. *Astronomy and Astrophysics*, Vol. 536, A16:1-14.
- [69] Wang L., Rowan-Robinson M. (2009) The Imperial IRAS-FSC Redshift Catalogue. *Monthly Notices of the Royal Astronomical Society*, Vol. 398:109-118.
- [70] Planck Collaboration VII. (2012) Planck Intermediate results. VII. Statistical properties of infrared and radio extragalactic sources from the *Planck* Early Release Compact Source Catalogue at frequencies between 100 and 857 GHz. *Astronomy and Astrophysics*, submitted; [arXiv.org//1207.4706v1](http://arXiv.org/abs/1207.4706v1).
- [71] Bethermin M., Dole H., Lagache G., Le Borgne D., and Penin A. (2011) Modeling the evolution of infrared galaxies: a parametric backward evolution model. *Astronomy and Astrophysics*, Vol. 529, A4:1-18.

- [72] Serjeant S., and Harrison D. (2005) The local submillimetre luminosity functions and predictions from Spitzer to Herschel. *Monthly Notices of the Royal Astronomical Society*, Vol. 356:192–204.
- [73] Oliver S.J., Wang L., Smith A.J., Altieri B., Amblard A., et al. (2010) HerMES: SPIRE galaxy number counts at 250, 350, and 500 μm . *Astronomy and Astrophysics*, Vol. 518, L21-L25.
- [74] Clements D.L., Rigby E., Maddox S., Dunne L., Mortier A., et al. (2010) Herschel-ATLAS: Extragalactic number counts from 250 to 500 microns. *Astronomy and Astrophysics*, Vol. 518, L8-L12.
- [75] Bethermin M., Dole H., Cousin M., and Bavouzet N. (2010) Submillimeter number counts at 250 μm , 350 μm and 500 μm in BLAST data. *Astronomy and Astrophysics*, Vol. 516, A43:1-15.
- [76] Puget J.L., Abergel A., Bernard J.P., et al. (1996) Tentative detection of a cosmic far-infrared background with COBE. *Astronomy and Astrophysics*, Vol. 308, L5-L9.
- [77] Hauser M.G., and Dwek E. (2001) The Cosmic Infrared Background: Measurements and Implications. *Annual Review of Astronomy and Astrophysics*, Vol. 39:249-307.
- [78] Dole H., Lagache G., Puget J.L., et al. (2006) The cosmic infrared background resolved by Spitzer. Contributions of mid-infrared galaxies to the far-IR background. *Astronomy and Astrophysics*, Vol. 451:417-429.
- [79] Soifer B.T., and Neugebauer G. (1991) The properties of infrared galaxies in the local universe. *The Astronomical Journal*, Vol. 101:354-361.
- [80] Planck Collaboration XVIII. (2011) Planck early results. XVIII. The power spectrum of cosmic infrared background anisotropies. *Astronomy and Astrophysics*, Vol. 536, A18:1-30.